

Review Article

Emission Mechanisms of Si Nanocrystals and Defects in SiO₂ Materials

José Antonio Rodríguez,¹ Marco Antonio Vásquez-Agustín,²
Alfredo Morales-Sánchez,³ and Mariano Aceves-Mijares²

¹ Instituto Superior Politécnico de Tecnología e Ciências (ISPTEC), Avenida Luanda Sul, Rua Lateral Via S10, Talatona, Belas, Luanda, Angola

² Department of Electronics, INAOE, 72840 Puebla, PUE, Mexico

³ Centro de Investigación en Materiales Avanzados S.C., Unidad Monterrey-PIIT, 66600 Apodaca, NL, Mexico

Correspondence should be addressed to Mariano Aceves-Mijares; maceves@ieee.org

Received 24 March 2014; Accepted 22 June 2014; Published 26 August 2014

Academic Editor: Anukorn Phuruangrat

Copyright © 2014 José Antonio Rodríguez et al. This is an open access article distributed under the Creative Commons Attribution License, which permits unrestricted use, distribution, and reproduction in any medium, provided the original work is properly cited.

Motivated by the necessity to have all silicon optoelectronic circuits, researchers around the world are working with light emitting silicon materials. Such materials are silicon dielectric compounds with silicon content altered, such as silicon oxide or nitride, enriched in different ways with Silicon. Silicon Rich Oxide or silicon dioxide enriched with silicon, and silicon rich nitride are without a doubt the most promising materials to reach this goal. Even though they are subjected to countless studies, the light emission phenomenon has not been completely clarified. So, a review of different proposals presented to understand the light emission phenomenon including emissions related to nanocrystals and to point defects in SiO₂ is presented.

1. Introduction

The luminescence of different silicon-based materials, such as hydrogenated amorphous silicon (a-Si:H) and silicon oxide (SiO₂), has been known for a long time. However, it was only after the finding of Canham [1] on strong visible room temperature photoluminescence (PL) from porous silicon (p-Si) that the development of efficient light sources based on silicon and related compounds was considered a real possibility. As a consequence, the establishment of a common silicon-based technological platform for opto- and microelectronic devices and the production of all-silicon optoelectronic circuits were envisioned. Beginning with the pioneer works related to this phenomenon, the origin of the emission was attributed to quantum confinement effects taking place in the silicon nanoparticles (Sinc) produced by electrochemical etching (nanocrystals or nanoclusters depending on the aggregation state, crystalline, or amorphous). The necessity to passivate the nanocrystal surface to eliminate nonradiative centers was also established. The passivation can be produced during the electrochemical process by a posttreatment under H₂

or by forming gas atmosphere via Si-H bonds (hydrides); it can also be achieved through a native oxidation process, under atmospheric conditions even for a short time, or by annealing it in an oxidizing atmosphere at an elevated temperature via different oxygen passivation configurations. As evidenced theoretically and experimentally, the emission mechanism and the properties of the emitted radiation significantly depend not only on the Sinc dimension, but also on the chemistry of the nanocrystal surface, being, in general, different for hydrogen and oxygen passivation. For applications, generally, the oxygen process is utilized. Therefore, the importance of a system formed by silicon agglomerates surrounded by amorphous SiO₂ (Sinc/SiO₂) as a basic material for light-emitting devices has been firmly established. Such a system, simply known as Silicon Rich Oxide (SRO), has been a matter of extensive research due to the transformation of agglomerates in nanocrystals and the emission taking place in the nanocrystals or around them.

An alternative mechanism of emission in SRO films, especially with low silicon excess, is related to point defects

in the SiO_2 matrix. The different chemical vapor deposition (CVD) techniques are naturally inclined to produce defects in the matrix of deposited materials. High temperature techniques, as low pressure chemical vapor deposition (LPCVD), are even more predisposed to such molecular changes. However, in spite of the defect formation when the mentioned techniques are used, it is uncommon to find studies that relate the emission with point defects in SRO.

The poor chemical and mechanical properties of p-Si stimulated the research work with other silicon-based luminescent materials during more than two decades. Among them are materials based on Sinc embedded in an SiO_2 matrix, which can be obtained by different techniques, such as Si^+ implantation into thermal SiO_2 , plasma enhanced chemical vapor deposition (PECVD), LPCVD, and Sol-gel. The Si nanostructures are then autoassembled from individual atoms under a high temperature annealing in an inert atmosphere. This process produces the Si diffusion, nucleation, and crystallization. Other Sinc/ SiO_2 -based materials are obtained by co-Sputtering, pulsed laser deposition (PLD), and oxidation of layers of Si nanoparticles synthesized from the gas phase. In the next section, some of the main synthesis techniques will be described.

So far, it has not been possible to find a physical model explaining the emission processes underlying all these Sinc/ SiO_2 -based materials. A good and unifying effort, in our opinion, is that of Koch and Petrova-Koch [2]. Instead, a rush of models (sometimes contradictory to one another) have been proposed to fundament this phenomenon for specific materials, obtained by specific techniques under concrete technological parameters. As a rule, a good agreement is reported between the results of the specific model and the experimental results for a particular material. It seems that these facts reflect a reality of nature; that is, intense luminescent radiation in a wide spectral range (from infrared to ultraviolet) can be produced in these materials following different physical mechanisms which will be reviewed in Section 3.

The intention of this paper is to review the mechanism of emission due to Sinc and the defects embedded in a dielectric matrix (SiO_2). In Section 2, we present some techniques commonly used to obtain SRO and related materials. In Section 3, a review of the different possible emission theories and defects is presented. We finish this section showing specifically the emission of off-stoichiometric oxide due to different excitation, which can be related to point defects.

2. Synthesis of Materials

The most extensive way to obtain silicon nanoparticles embedded in dielectric layers, either silicon oxide or nitride, is through the segregation of the excess silicon atoms in silicon enriched layers with a thermal annealing at a high temperature [3, 4]. Here, the technological parameters such as the duration of the thermal treatment, the annealing temperature, and the Si excess content all determine the final

size of the particle, the size dispersion, and its nature either amorphous or crystalline. However, different techniques are also used to produce Sinc/ SiO_2 -based materials.

2.1. Porous Silicon (p-Si). Porous silicon was discovered by Uhlir at the Bell laboratories (US) in 1956 [5]. Despite this early discovery, the scientific community was not interested in p-Si until the late 80s, when Canham proposed that p-Si could display quantum confinement effects [1]. In his published experimental results, strong light emission from silicon was obtained after subjecting the Si-wafers to an electrochemical and chemical dissolution. Different PL peaks were observed depending on the porosity of the layer. These novel results stimulated the interest of the scientific community in the study of the nonlinear optical and electrooptical properties of silicon, especially due to their potential applications. Despite the strong room temperature luminescence observed in p-Si, it was found that it suffers from poor mechanical and chemical stability producing degradation in the PL properties [6, 7]. Multiple studies have been done to overcome this limitation such as modifications introduced in the etching procedure [8, 9]. Some authors have reported that a postetching treatment in H_2O_2 leads to a decrease of the nanoparticle core size and also, to some extent, changes the surface oxide for the modulation of the photoluminescence color [8].

2.2. Ion Implantation. In the ion implantation technique, a thermal silicon oxide grown on a silicon wafer is implanted with silicon ions at a specific dose and energy. With this technique, both chemical and structural changes are introduced by the implanted ions. To activate the implanted ions and to repair the damage produced, a thermal annealing is necessary. In the case of Si ions implanted into silicon dioxide matrix, a silicon agglomeration in the form of silicon nanoparticles is obtained after the thermal annealing process. The dose and energy of implantation determine the silicon excess and the depth profile, respectively [10–13]. In some cases, multiple silicon ion implantations are used to obtain a uniform depth profile of silicon excess and a uniform Sinc density [10].

2.3. Chemical Vapor Deposition (CVD). There are a great number of forms of CVD. These processes differ by the means in which chemical reactions are initiated (e.g., activation process) and process conditions. In a typical CVD process, the wafer or substrate is exposed to one or more volatile precursors, which react and/or decompose on or near the substrate surface to produce the desired deposit. The main CVD techniques used for Sinc fabrication are LPCVD and PECVD. SRO films are easily deposited by PECVD and LPCVD techniques using oxidant species like nitrous oxide (N_2O) and silicon compounds (i.e., silane, SiH_4) as reactant gasses [14–17]. For these techniques, Si excess in the deposited

films is controlled by a parameter R_o defined by (1), which relates to the flux of the reactant gases N_2O and SiH_4 ;

$$R_o = \frac{F(N_2O)}{F(SiH_4)}. \quad (1)$$

After SRO films are thermally annealed at a high temperature, a phase separation occurs between Si and SiO_2 creating Si agglomerates that can be nanocrystalline or not. Again, the Sinc formation and size depend on the silicon excess inside the deposited films, as well as the time and the temperature of thermal annealing.

For LPCVD, SRO is deposited at subatmospheric pressures and at a temperature of around $700^\circ C$ [14, 15]. Reduced pressures tend to reduce unwanted gas-phase reactions and improve film uniformity across the wafer. Meanwhile, SRO-PECVD utilizes a radio frequency (RF) discharge to enhance the chemical reaction rates of the precursors [16, 17]. PECVD processing allows deposition at lower temperatures, typically $300^\circ C$, which is often critical in the manufacturing of semiconductors.

2.4. Sol-Gel. Sinc/ SiO_2 -based materials are also obtained through the synthesis of SRO films by the Sol-gel method using triethoxysilane (TEOS) or the innocuous hexaethoxydisilane (hexaet) and hexamethoxydisilane (hexamet) monomers followed by a subsequent thermal treatment [18–20]. In the last case, the mentioned precursors (hexaet or hexamet) are mixed with ethanol and subsequently diluted with acidic water. The resulting solution is stirred in a sealed disposable beaker. The polymer is condensed and then dried in an annealing furnace at a low temperature. These SRO films are thermally annealed at a high temperature to obtain the silicon nanoparticles [20]. Through this method, it is also possible to control the PL spectra by varying the parameters of the technological process [18–20].

2.5. Sputtering. In this technique, plasma is created and the ions from this plasma are accelerated into a source target material etching it. If the sample surface is placed next to the target or in the path of the sputtered atoms, they will collide and eventually be adsorbed onto the sample forming a thin film.

To deposit SRO films, SiO_2 and Si targets are used. The amount of silicon excess can be controlled by adjusting the ratio at which each target is sputtered [21]. The low deposition rate has made this technique proper for obtaining superlattice structures and for the engineering of band gaps for silicon-based materials [21–23].

3. Emission Mechanisms

In this study, the materials based on the system Sinc/ SiO_2 , that is, silicon nanocrystals either embedded in a SiO_2 matrix or capped by SiO_2 shells, will be discussed. A rush of models has been proposed to explain the experimental results of the interaction of light (absorption and luminescence) with these materials. In the next sections, an insight into these

models will be explored based on published works. We will focus separately on the mechanisms related to Sinc core, to Sinc/ SiO_2 interface, and to SiO_2 matrix. Then a review of known Si–O emissive defects in silica is presented. Finally the emission related to such defects is linked specifically to SRO obtained by LPCVD.

3.1. Sinc Core Related Emission: Quantum Confinement Effect. The strong visible luminescence, first observed by Canham [1] in porous silicon and subsequently obtained by other researches in different Sinc/ SiO_2 -based materials, has been explained by a model based upon the quantum confinement or quantum size effect [1, 24, 25]. Theoretical evidence was established by Delerue et al. [26] under the frame of the linear combination of the atomic orbitals (LCAO) technique. Given that silicon is an indirect-gap semiconductor, the phonon-assisted radiative recombination is very inefficient. Moreover, as its gap at room temperature is around 1.1 eV, visible emission is precluded. A different scenario is encountered by reducing the particle dimensions under a few nanometers. When the nanostructure diameter (crystallite or cluster supposed spherical) is less than the size of the free exciton Bohr radius, 4.3 nm in bulk c-Si [27], the quantum size effect takes place; the electronic levels, which exhibit a quasi-continuous spectrum for bulk materials, become discrete and the effective band gap enlarges as the diameter (d) is reduced (Figure 1). In this case, such 0-dimensional nanostructures are called “quantum dots” and their physical features are described by the classical text book “particle in a box” scheme. In this diameter range, the band gap increases according to an approximate d^{-2} law, the oscillation strength increases, and the radiative lifetime varies from a millisecond to a nanosecond, as calculated in the frame of an effective-mass approximation [28]. However, the more precise considerations of Delerue et al. [26] allowed obtaining a $d^{-1.39}$ behavior for small enough particles, with the energy gap of silicon nanoparticles (E_g) being calculated through the following semiempirical expression:

$$E_g \text{ (eV)} (d) = E_{g0} \text{ (eV)} + \frac{3.73}{d(\text{nm})^{1.39}}, \quad (2)$$

where E_{g0} is the energy gap of bulk silicon. According to this model, the emission spectrum can be tuned from infrared to blue by reducing the structure diameter if the particle surface is passivated with Si–H bonds, a fact experimentally observed by Gupta et al. [29]. Figure 2 depicts a comparison of theoretical and experimental results as reported by Garrido et al. [30] on ion beam synthesized Sinc in SiO_2 . In this figure, the experimental results obtained by these authors for band gap, as obtained from photoluminescence excitation measurement and photoluminescence peak position, are contrasted and agree well with the behaviors theoretically calculated by Delerue et al. [26], Wang and Zunger [31], and Takagahara and Takeda [28].

Another example of Sinc core-related emission is observed in Figure 3. The photoluminescence spectra obtained for Sol-gel SRO annealed one hour in N_2 atmosphere at different temperatures are depicted. The

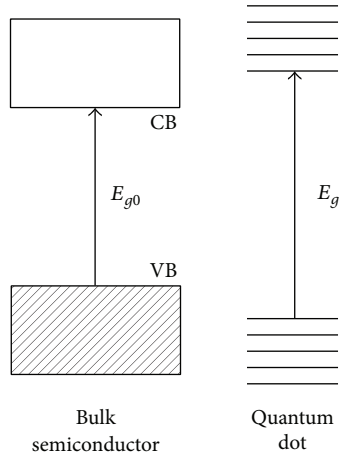


FIGURE 1: Diagram illustrating the effect of quantum confinement in the energy band structure.

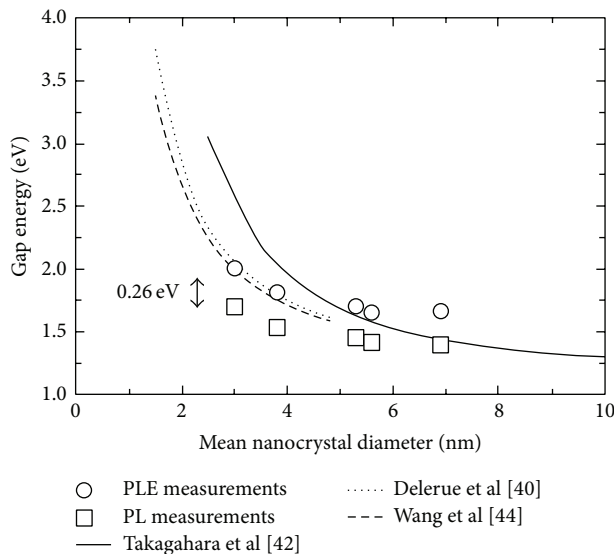


FIGURE 2: (Figure 14 from [30]). Theoretical (solid, dotted, and dashed lines) and experimental (circles) data for the band gap energy as well as experimental PL peak energies (squares) as a function of nanocrystal diameter. The double arrow indicates the value of the Stokes shift.

as-synthesized samples are obtained as described in epigraph 2 by using a hexaethoxydisilane monomer as a precursor. The dramatic increase of PL intensity for annealing temperatures in the range of 1050–1100°C corresponding to crystallization of the Sinc as well as the redshift of maximum PL for increasing annealing temperature and time is observed. This fact corresponds to an increase of Sinc diameter according to the quantum confinement effect. The crystalline nature of the Sinc was verified by Raman shift measurements as indicated in Figure 4.

Unfortunately, the simple behavior just described is not always observed in Sinc/SiO₂ materials. Important discrepancies with this simple picture have been encountered in practice and will be raised later.

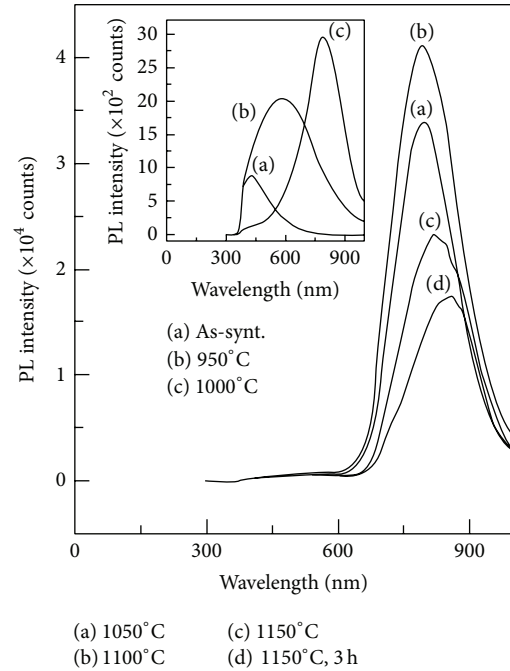


FIGURE 3: (Figure 1 from [20]). PL spectra for Sol-gel SRO (hexaet-based), annealed for one hour (if not specified), at increasing temperatures. Low intensity curves are separately shown in the inset for clarity.

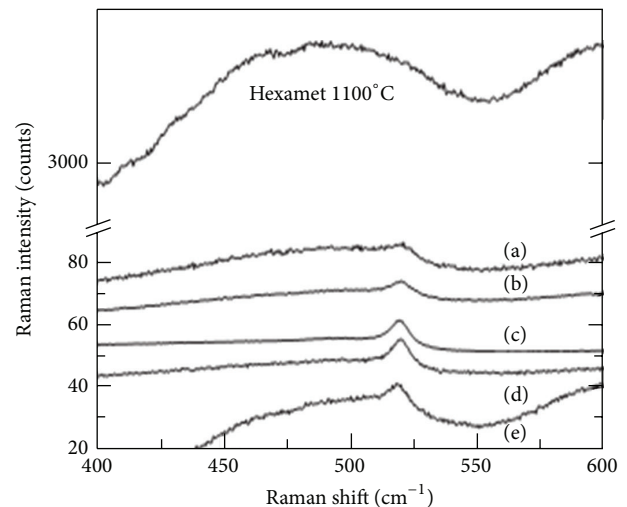


FIGURE 4: (Figure 4 from [20]). Raman shift spectra for some of the samples as in Figure 3. Curves (a)–(d) correspond to the samples treated at 1050, 1100, 1150, and 1150°C (3 h), respectively. Curve (e) is from a SRO obtained from a mixture of hexamet and hexaet. A curve for a pure hexamet-based sample is also shown.

Another consequence of the quantum confinement is the dramatic increase of the radiative recombination efficiency. In quantum confined systems, the extremely reduced dimensions lead to a major spread of the wave vector value in the reciprocal space according to the uncertainty principle, thus

producing a relaxation of the moment selection rule and the possibility of zero-phonon direct radiative optical transitions.

Qualitatively, the confinement due to reduced particle size produces an increase of the overlap between electron and hole wave functions in k -space, which leads to an increase of the radiative recombination probability. Moreover, as size is reduced, the probability of finding a nonradiative recombination center in the particle decreases provided that the particle surface is appropriately passivated. This is based on Sinc embedded in silicon oxide or other dielectrics, such as a silicon nitride matrix with a higher band gap, thus producing a quantum well. Consequently, carrier diffusion from the particle towards external nonradiative recombination centers is avoided. The mentioned facts lead to the photoluminescence increase from Sinc few orders of magnitude larger than for bulk silicon, as experimentally observed.

Attributing the emission phenomenon in Sinc/SiO₂ systems to direct optical transitions has been somewhat controversial. Indeed, lines of evidence on zero-phonon as well as on TO phonon-assisted transitions were encountered by Sychugov et al. in their studies of oxidized Si quantum dots emission by single-dot luminescence spectroscopy [32]. Furthermore, Garrido et al. [30] argued that the dominant mechanism of emission for their ion beam synthesized Sinc embedded in SiO₂ is a fundamental (indirect) transition located at the interface Si/SiO₂ with the assistance of a local Si–O vibration. The first observations on direct transitions in Sinc-based materials were those from Wilcoxon et al. [33] in their research on the optical and electronic properties of Si nanoclusters synthesized in inverse micelles.

Moreover, there is proverbial uncertainty reported in the literature relating to the determination of the size and the size distribution of nanocrystals from electron microscopy due to a low contrast between Si and SiO₂. This has been a main drawback in establishing a stable correlation between structural and optoelectronic properties of Sinc embedded in SiO₂, which has led to ambiguities in determining the emission mechanisms. However, in the paper of Garrido et al. [30], a successful method was explored for imaging Sinc in SiO₂ matrices by using high-resolution electron microscopy in conjunction with conventional electron microscopy in dark field conditions.

On the other hand, the quantum confinement effect is not always observed in practice for Sinc/SiO₂-based materials. According to this model, a blueshift of the PL energy peak should take place as the diameter of the nanoparticles decreases in the range of few nanometers. However, not only a blueshift but also a redshift should occur [34], and no dependence on this parameter has been observed [35–37]. In addition, a redshift of PL spectrum as large as 1 eV has been observed after exposure to oxygen in porous silicon quantum dots [38], and a discontinuity at about 590 nm of PL spectral behavior with reducing size has also been reported [8, 38]. These discrepancies may be understood by considering that the PL spectra in Sinc/SiO₂-based materials are really the result of, besides the quantum confinement effect, the simultaneous action of various other emission mechanisms [34]. Most of these are based on models which attribute a key role in the luminescence phenomenon through

the interface between the Sinc and the dielectric matrix. Such are the cases of emission due to exciton confined in the Sinc/SiO₂ interface [35, 39] and the emission through carrier energy levels introduced in the quantum dot band gap by surface Si=O bonds (nonbridged oxygen passivation) [8, 38, 40], by defects in the silicon suboxide (SiO_x) or silicon oxide shell surrounding the nanocrystal [41], or by surface states generated in the perturbed Si-bonded to O and H [2]. Other luminescence mechanisms have been associated with structural defects of the silicon oxide matrix [36] or with different silicon-based chemical species like siloxane (Si₃O₃H₆) [42] and polysilane (SiH₂)_n [43]. In the next epigraphs, the luminescence mechanisms related to Sinc/SiO₂-matrix interface (surface confined excitons, surface carrier energy levels introduced by passivant bonds or by perturbed crystalline Si structure) and oxide matrix defects will be considered.

3.2. Emission Mechanisms Related to Sinc/SiO₂ Interface.

Among the rush of works and models published after Canham's, we distinguish a line of continuity and development beginning with the pioneers papers through Kanemitsu et al. [35, 39] and Kanemitsu [44], and those from Koch and Petrova-Koch [2], Wolkin et al. [38], Wilcoxon et al. [33], Nishida [45], and Dohnalová et al. [8]. In [35] the authors report the results of their research work on free-standing p-Si thin films formed by nm-sized Si crystalline spheres dispersed in an amorphous phase. In [39] the authors study nm-sized spherical Sinc obtained by synthesis from vapor phase and subsequently oxidized. The experimental results of both papers suggest that the photogeneration of carriers occurs in the Sinc core, where the band gap is modified by the quantum confinement effect, while the strong PL (size-independent, ~1.65 eV) (see Figure 5) comes from the near-surface region of small crystallites. They proposed a three-region model (Figure 6) in which the Sinc core is surrounded by a shell of amorphous silicon oxide (a-SiO₂) and a transition interfacial layer. The composition of this intermediate layer corresponds to a nonstoichiometric silicon oxide (SiO_x, $x < 2$), and its band gap energy is lower than that of the Sinc core for core diameters ≤ 5–7 nm. According to the model, the carriers photogenerated in the core diffuse through a thermally activated mechanism towards this interfacial region, where the intense PL radiation is produced via two-dimensional confined excitons. The observed temperature dependence on the PL intensity unambiguously confirms this proposition. These arguments also explain the increase of PL intensity as the crystallite diameter is reduced. In this case, the efficiency of carrier diffusion from core to near-surface layer as well as the excitons' confinement also increases. In the paper [39], the authors explicitly refute the possibility that the emission takes place via localized states, as the states usually act as nonradiative centers.

The next report from Kanemitsu in 1994 [44] was devoted to the same material system seen in [39] (oxidized spherical Sinc obtained by synthesis from vapor phase) with a mean crystallite diameter of 3.7 nm. A time-resolved PL study was accomplished. Also, PL spectra under weak continuous wave

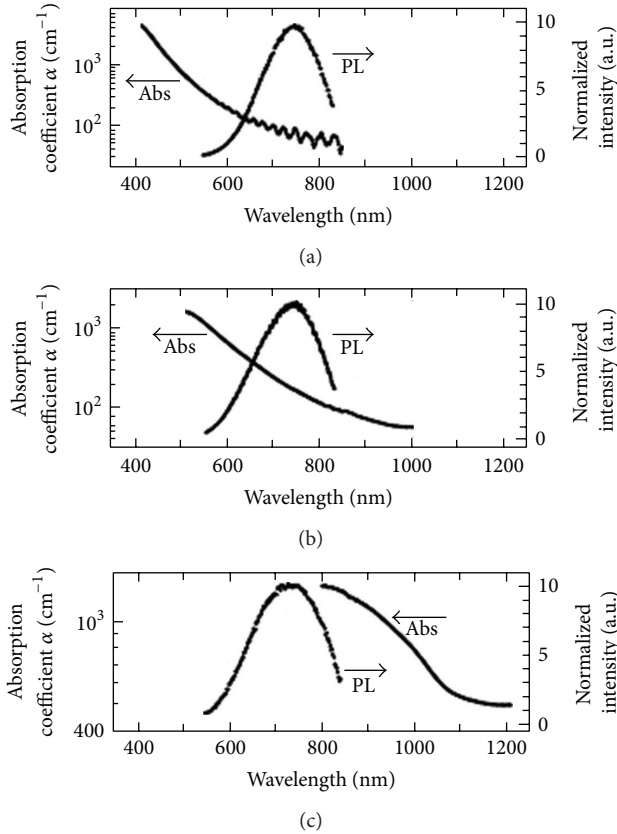


FIGURE 5: (Figure 4 from [35]). Absorption and PL spectra of p-Si films: (a) $d \sim 2$ nm, (b) $d \sim 3.5$ nm, and (c) $d \sim 9$ nm.

(cw) excitation as well as time averaged PL spectra under intense and weak pulsed-laser excitation were obtained. Reference was made neither to the interfacial region nor to the emission mechanism through two-dimensional confined excitons; rather, the emissions were associated with surface localized states.

Figure 7 summarizes the results of optical absorption and PL spectra under cw and pulsed-laser excitation. A weak absorption tail in the visible region and a strong absorption above 3 eV are observed. Furthermore, in continuous excitation, a strong, stable, broad (~ 0.3 eV full width at half maximum, FWHM, Gaussian-like shape), slow (microsecond order), and nonexponential decay (stretched exponentially instead) red band (~ 760 nm) is obtained. According to its properties, this band is associated with the hopping of carriers among the localized surface states (the energy levels of which form a band tail), from the high energy levels to the low energy ones, followed by radiative recombination through the band gap of these surface regions. This proposition is supported by the *ab initio* calculations of Takeda and Shiraishi [46], who obtained a value of 1.7 eV for the band gap of a completely oxidized Si sheet very similar to the Sinc surface in the Sinc/SiO₂ system. This value roughly coincides with the spectral position of the red PL band. Under short pulsed excitation, a new fast nonexponential decay blue-green band emerges in addition to the red one. The intensity of this band

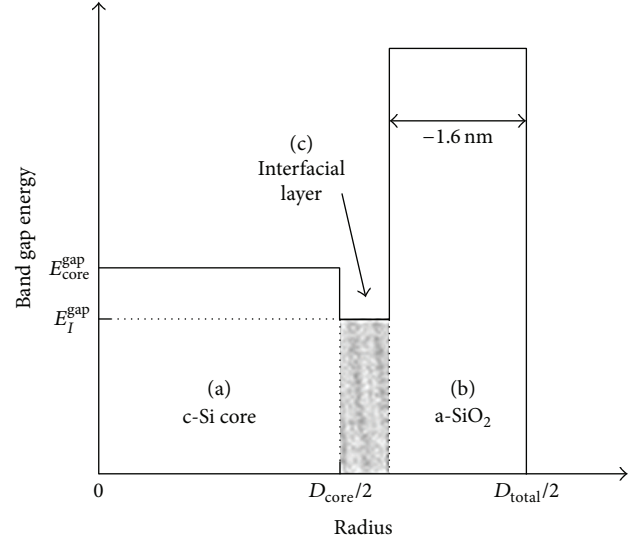


FIGURE 6: (Figure 4 from [39]). Energy gap diagram of the three-region model proposed by Kanemitsu et al.

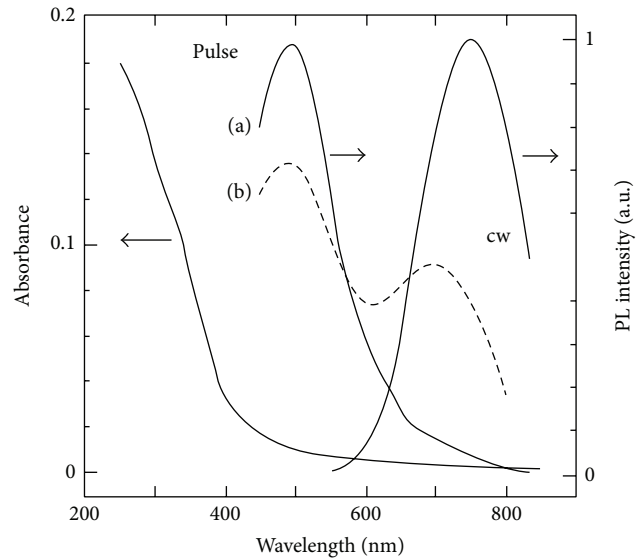


FIGURE 7: (Figure 1 from [44]). Optical absorption spectrum, PL spectrum under cw 325 nm laser excitation, and the first 200 ns averaged PL spectra under 5 ns, 335 nm pulsed laser excitation of (a) $\sim 100 \mu\text{J}/\text{cm}^2$ (solid line) and (b) $\sim 0.6 \mu\text{J}/\text{cm}^2$ (broken line) at room temperature.

increases with the excitation intensity and eventually the red band disappears. Its spectral position roughly agrees with the band gap energy (2.4 eV) of a 3.7 nm Sinc [28]. Therefore, its origin is attributed to carrier radiative recombination in the Sinc core. Its appearance has been considered a result of the saturation of the localized surface states' population when the material is excited by short and energetic laser pulses. It is due to the low density of states and the large recombination lifetime (microsecond order) of localized states. Under these excitation conditions, part of the photogenerated carriers

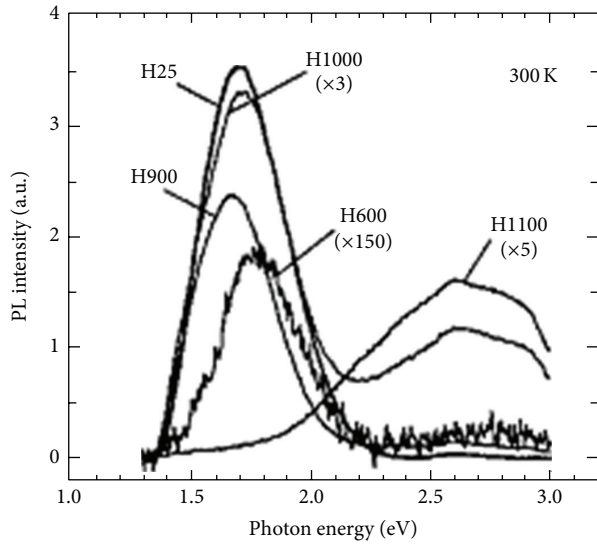


FIGURE 8: (Figure 2 from [2]). Room temperature PL spectrum of a set of thermally oxidized p-Si samples (rapid thermal oxidation, 30 s). H25 is the as-prepared sample. The others have been treated at the temperature indicated. The diameter of the Sinc decreases when the oxidation temperature is increased.

stays in the core and recombines there, thus producing the so mentioned blue-green band.

In 1996, based on experimental results, Koch and Petrova-Koch [2] tried to establish a model accounting for the properties of the most studied Sinc-based luminescent materials reported to date, that is, hydrided and oxidized p-Si, oxidized Sinc synthesized from a gas phase and ion beam synthesized Sinc in SiO_2 . In this, and in other related papers [47–49], they followed a surface state model, somewhat similar to that of Kanemitsu in [44]. In this model, the absorption (carrier generation) took place in the Sinc core following the quantum size effect but the recombination occurred via localized defect states in the passivated surface layer. The size effect was observed in the PL spectra for hydrided p-Si. For the oxidized one, the pinning of the PL energy peak in the range of 1.5 eV–1.7 eV as well as the discrete emergence of a fast blue band was observed as the diameter of the Sinc decreased due to increased oxidation temperature (see Figure 8).

Figure 9 shows the behavior of Si^+ implanted SiO_2 and annealed in forming gas. Observe the continuous redshift of the PL peak energy as the annealing time increases in correspondence with the growth of the Sinc. This behavior is not explained here according to the conventional quantum confinement effect for recombination that takes place in the Si core. Rather, the mentioned surface state model is adopted. Sincs larger than about 1.5 nm are considered as a central crystalline core formed by perfect Si-tetrahedra and a surface layer with thickness of the dimension of a Si unit cell formed by Si-tetrahedra, which are perturbed due to bonds with other matrix atoms. As a result, a spectrum of disorder-induced states is formed in this region, with energies lower than the states in the unperturbed core. Therefore, excited electrons and holes localized recombine in this layer. As the

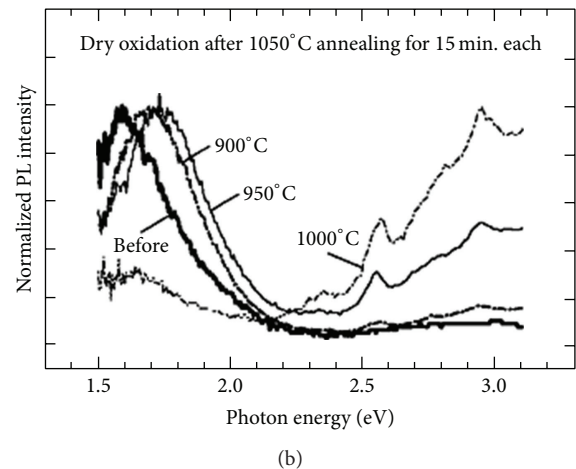
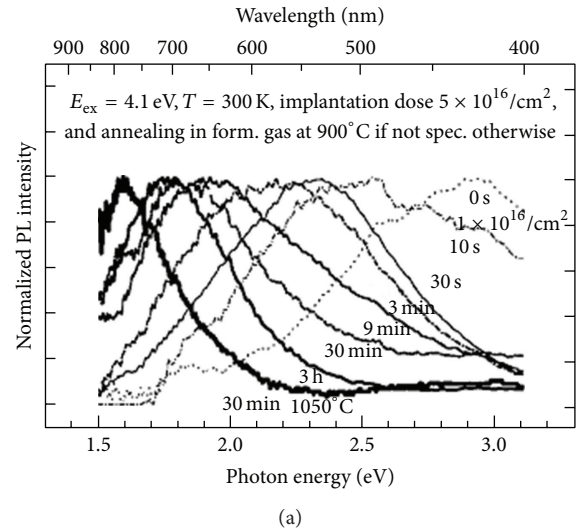


FIGURE 9: (Figure 3 from [2]). PL spectra for Si^+ implanted SiO_2 , annealed at high temperature in forming gas, for increasing annealing time (a) and isochronal (15 min) dry oxidation of the samples annealed at 1050°C in forming gas for increasing oxidation temperature (b).

nanocrystals grow, the increased separation of the electron-hole pair implies a lower PL energy and a longer lifetime, in agreement with the experiment.

The PL spectra obtained after subsequent isochronal dry oxidation at different temperatures from the samples previously annealed at 1050°C for 30 min are also depicted in Figure 9 (lower half). As the oxidation temperature increases, that is, as the diameter of the Sinc is reduced, the PL peak energy pins around 1.6–1.7 eV (slow decay red band) until it finally vanishes with the simultaneous emergence of the fast decay blue band in complete analogy with the behavior of oxidized p-Si (Figure 8). The origin of this fixed energy red band is easily explained within the frame of the same surface state model. In this case, the emission occurs in an interfacial SiO_x ($x < 2$) layer formed at the oxidation front, where the authors assume localized defect-type of states to explain the fixed energy at around 1.7 eV. Therefore, the authors compared their model with the three-region model

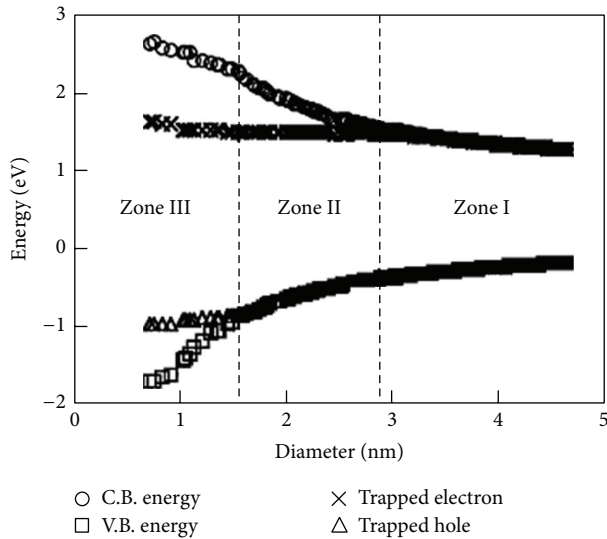


FIGURE 10: (Figure 3 from [38]). Calculated energy band structure in Si nanocrystals, as a function of cluster size and surface passivation. Trapped electron and hole states according to diameter values are observed.

of Kanemitsu et al. [35, 39] but argued about the difficulty to imagine an interfacial SiO_x ($x < 2$) layer with a band gap lower than that of the Si-crystallite. No mention is made of Kanemitsu's report [44], where the origin of the red fixed band is associated with surface localized states. The origin of the blue band is not discussed in the paper, and rather the reader is remitted to [50].

An important clarification of the Sinc/ SiO_2 surface-related emission mechanism was presented in 1999 by Wolkin et al. [38] regarding their results on silicon quantum dots in p-Si. These authors analyzed experimentally the PL emission from the p-Si in a range of dot diameters below 5 nm for two groups of samples: one of them remained at all times in an Ar (oxygen-free, hydrogen passivated) atmosphere and the other one was exposed to air (oxygen passivated) after the etching procedure. They also developed a theoretical model which shows the presence of new carrier states in the band gap of the smallest quantum dots when the Si=O bonds are formed. As seen in the framework of their model, Figure 10 depicts the calculated energy band structure in Si nanocrystals as a function of cluster size and surface passivation. On the other hand, Figure 11 shows the theoretical results for free exciton band gap energy (upper line) and for the lowest transition energy in the presence of a Si=O bond (lowest line) as a function of crystallite diameter. The experimental room temperature PL peak energies for both the aforementioned groups of samples, oxidized and not oxidized (hydrogen passivated), are also depicted in this figure. A good agreement between experiment and theory is observed. In addition, the effect of oxidation depends on the crystallite size; three different zones with different emission mechanisms may be distinguished. For crystallites with diameters larger than about 3 nm (zone I), even when the samples are oxidized or

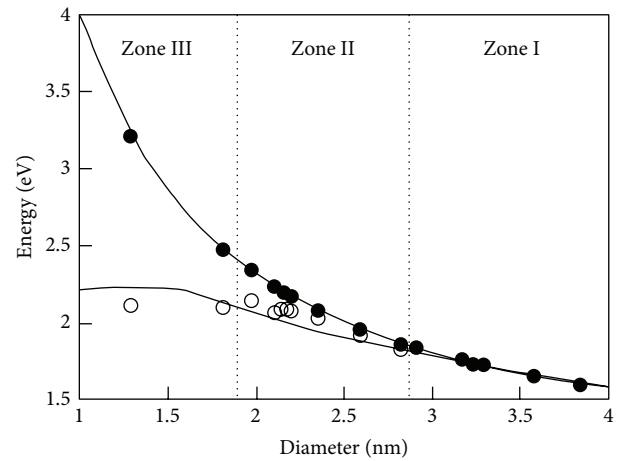


FIGURE 11: (Figure 4 from [38]). Theoretical results for the free exciton band gap energy (upper line) and for the lowest transition energy in the presence of a Si=O bond (lowest line) as a function of crystallite diameter. The experimental room temperature peak PL energies for both the oxidized (○) and the nonoxidized or hydrogen passivated (●) samples are also depicted.

not, the PL peak energy increases with decreasing nanocrystal sizes; the emission involves free excitons and the scenario corresponds to the quantum confinement effect. This is the area generally covered by most of the published works which corresponds to the PL spectrum in the orange-red zone. For diameters lower than about 3 nm, the emission corresponds to transition from a trapped electron state to a valence band (zone II) or from a trapped electron state to a trapped hole state (trapped exciton) (zone III). These results explain the significant Stokes shift for the smallest nanocrystallites [38], the pinning of the PL spectra at about 2.1 eV (590 nm) with decreasing crystallite diameters [8, 38], and a PL spectrum red shift as high as 1 eV for p-Si samples after exposure to air [38].

An apparent contradiction between this model and those from Kanemitsu et al. and Koch et al. deserves attention. In these last models, it was firmly established that when a Sinc-based luminescent material is oxidized at a high temperature so as to reduce the Sinc size below a few nm, no matter what is its method of synthesis, the PL peak pins at about 1.6-1.7 eV. However, according to Wolkin's results for p-Si with decreasing Sinc size the PL spectra pin at about 2.1 eV after oxidation at room temperature in air or pure oxygen atmospheres. These different behaviors might be associated, in our opinion, with differences in the oxygen passivation configurations [51] produced by different oxidation conditions (room or high temperature oxidation), leading to different oxidation-related energy band structures. In Figure 12, we reproduce Figure 5 from the paper by Nishida [45]. In his paper, the author theoretically examined the effect of the configuration of oxygen on the electronic structure of a Sinc in order to clarify the mechanism of the oxidation-induced redshifts in the PL spectra for H-covered p-Si. Nishida consistently calculated the electronic state of

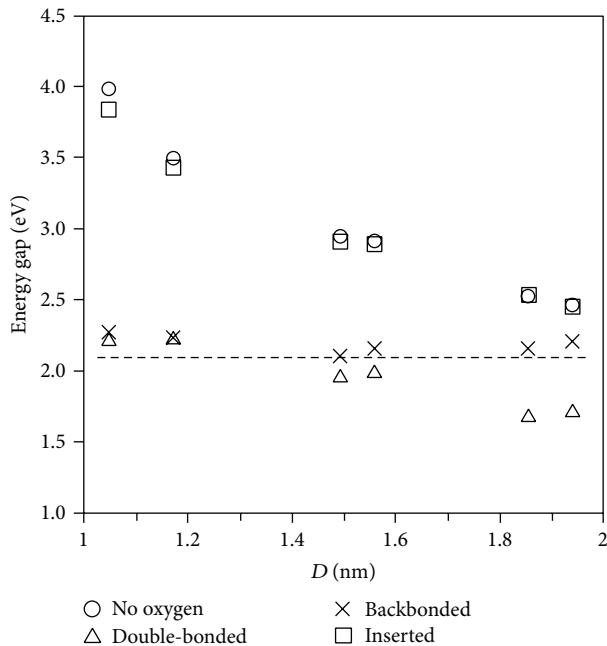


FIGURE 12: (Figure 5 from [45]). Calculated HOMO-LUMO energy gaps as a function of the Sinc diameter (D) for double-bonded, backbonded, and inserted oxygen configurations in comparison with the unoxidized case and with the oxidation-induced peak energy at ~ 2.1 eV in the PL spectra observed in p-Si.

Sinc with diameters 1-2 nm by using the extended Huckel-type nonorthogonal tight-binding (EHNTB) method for three possible oxygen configurations: (i) double-bonded, (ii) backbonded, and (iii) inserted. Figure 12 shows the calculated HOMO-LUMO energy gap as a function of the Si dot diameter (D), in comparison with the case for the unoxidized Si dots and with the oxidation-induced peak energy at ~ 2.1 eV in the PL spectra observed in p-Si. As observed, the energy gaps calculated for the backbonded oxygen configuration in all Si dots studied coincide well with the observed PL-peak energy whereas those calculated for the double-bonded oxygen configuration gradually decrease from 2.2 eV up to about 1.7 eV with the increase in dot size in the range of 1-2 nm. This last value resembles those from Kanemitsu's and Koch's results for Sinc diameters higher than 3 nm. In view of the precedent arguments, one is tempted to explain the mentioned contradiction as follows: for oxidation at high temperature, which reduces the Sinc diameter as in the works of Kanemitsu et al. and Koch et al., the backbonded oxygen configuration is observed. For room temperature oxidation, however, a double-bonded oxygen configuration is obtained.

The experimental results for PL peak energy as a function of nanocrystal diameter for the Sinc-based materials are summarized by Wilcoxon et al. in their paper of 1999 [33] on optical and electronic properties of Si nanoclusters synthesized in inverse micelles. Figure 13 reproduces Figure 10 of that paper, where the results of their own work as well as the data from the literature are depicted. The first observation made by the authors is the different dependences on size reported by the different papers. This fact is partially attributed to

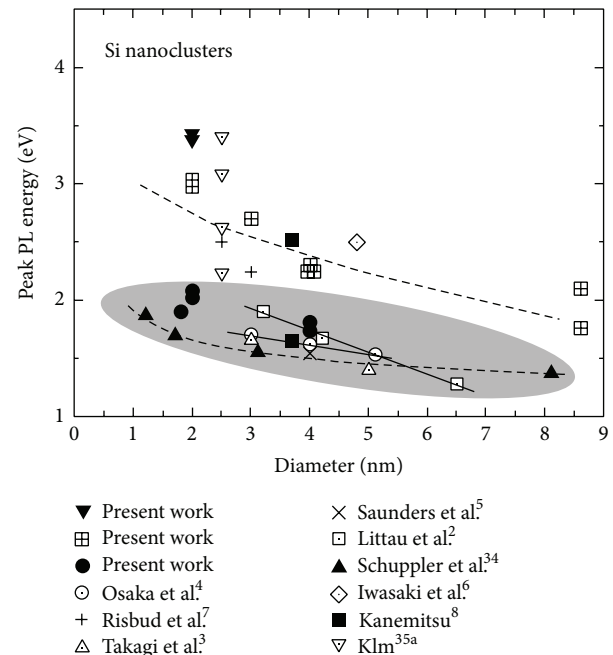


FIGURE 13: (Figure 10 from [33]). Summary of experimental data (from reference [33] and from papers previously published and referenced in [33]) on peak PL energy versus Si nanocluster size.

uncertainties in size. The exciton binding energy (as high as ~ 350 meV as reported by [33]) might also have importance in the different values reported. Furthermore, all PL peaks of SiO_2 -capped Sinc or Sinc embedded in glass matrices fall into the shaded region of the diagram while the experimental data for the oxygen-free samples (at the same value as the diameter) fall above this shaded region. So, it can be clearly concluded that the interface situation plays a significant role in the luminescence response for these materials.

Let us finally pay attention to the discrete fast (F) blue band appearing in the PL spectra of Sinc-based materials jointly with the slow (S) red one when reducing Sinc size as seen in the paper from Dohnalová et al. [8]. As was mentioned before, both bands were observed in the work from Kanemitsu [44] for oxidized spherical Sinc obtained by synthesis from the vapor phase excited under short intense pulsed laser radiation and in that from Koch and Petrova-Koch [2] for thermally oxidized p-Si as well as for oxidized Sinc (thermally segregated from Si^+ -implanted SiO_2). In the first paper, the origin of the F-band was attributed to fundamental carrier recombination in the crystalline core of their 3.7 nm oxidized Sinc. In the second one, the reader is reminded to [50] for an explanation of the origin of the blue band. However, the explanation in the last reference is not clear. This last paper is just devoted to the study of the fast and slow visible luminescence bands of oxidized p-Si; however, at the end, the authors confessed that the work does not resolve the questions as to how the red and blue PL originate.

A detailed analysis of the point is realized in [8] for p-Si with a high porosity obtained through a modification of Si-wafer electrochemical etching. In particular, the use of an

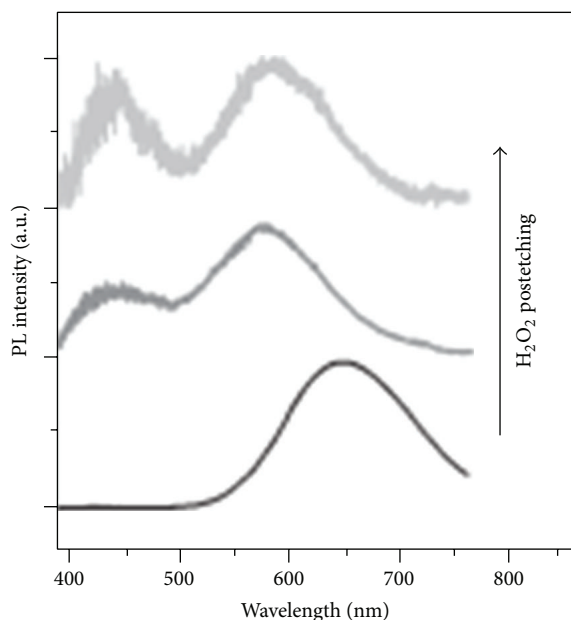


FIGURE 14: (Figure 1(b) from [8]). General behavior of the continuous wave excited PL spectra as the Sinc size decreases for high porosity aged (oxidized) p-Si, obtained through the use of a H_2O_2 postetching, to reduce the Sinc diameter.

H_2O_2 postetching (to reduce the Sinc diameter) is studied via the time-resolved PL spectroscopy. The authors developed a series of experiments starting with the electrochemical etching and applying an increasing H_2O_2 postetching with the corresponding reduction in the Sinc size: the so-called standard (no postetching), yellow, white, and blue samples. No measurements of the real sizes are reported. The emission study is performed after the samples are aged (oxidized); the color of the standard sample, for instance, is changed from green to orange-red in this process. In their paper [8], the authors survey the treatment of both bands in the literature, thus verifying that most published papers deal separately with either the F- or the S-bands which preclude any analysis about the possible relationship between both emission mechanisms. Figure 14 reproduces Figure 1(b) from paper [8] which shows the general behavior of the continuous wave excited PL spectra as the Sinc size decreases. The results can be summarized as follows: a red slow (S) band appears on the microsecond timescale. This band blueshifts but stops at about 590 nm. Simultaneously, a blue fast (F) band emerges in the nanosecond timescale, whose relative intensity (relative to the S-band which finally fades away) increases. Therefore, a discontinuity in the spectral blueshift occurs as Sinc size is reduced, which is attributed to switching between S- and F-band emissions.

The authors declare as consensus that the origin of the S-band is the result of recombination through quantized states in relatively large Sinc in cooperation with the surface passivation species. Figure 14 represents the ideas of the basic models described above. In our opinion, this band is also related with relatively small Sinc. The PL spectra, which redshift and pin at about 590 nm, are due to oxidation,

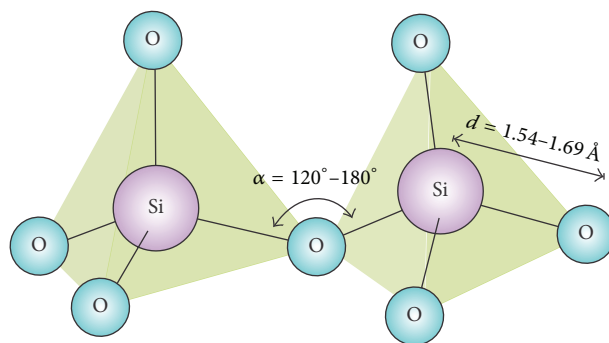


FIGURE 15: Ideal representation of silicon dioxide; the oxygen joining two silicon atoms is a bridging atom.

according to the model of Wolkin et al. [38]. Moreover, the authors declare, a priori, that there is no obvious reason why the blueshift of the S-band should stop at the “magic” 590 nm boundary rather than continue up to blue and argue that the only plausible reason would be that the Sinc reached its smallest possible size. This argument ignores the same phenomenon of the pinning of the PL spectra just at this spectral position (590 nm or 2.1 eV) for aged p-Si [38]. They also analyzed the abrupt switching from one emission mechanism (S-band) to another (F-band) and proposed a model based on spatial restructuralization; that is, the Sinc changes from a crystalline to an amorphous state for very small sizes with the corresponding changes in optical properties.

Finally, the authors analyzed the controversial origin of the F-band with their experimental results. Different possible radiative channels have been discussed in relation to previously published works; a prevailing view is that luminescent defect states are localized in the interface $\text{Sinc}/\text{SiO}_x\text{-SiO}_2$ (please, consult directly the paper for details). However, they support that the F-band is due to a quasi-direct radiative recombination inside the Si nanoparticles’ (nanocrystals or nanoclusters) core, in correspondence with Kanemitsu’s proposition [44].

3.3. SiO_2 Defect-Related Emission: Point Defects. It is well known that the color of gemstones is determined by the light absorption, reflection, or emission of intrinsic or extrinsic defects in natural oxides. Nowadays, the point defects or color centers are relevant in understanding the emissive properties of materials that have a variety of applications in our high technology lifestyle. Silicon dioxide, in its different forms including quartz and off stoichiometric oxide, has been studied because it can be used to produce light. Ideally, SiO_2 is a continuum arrangement of silicon surrounded by four oxygen atoms forming tetrahedrons, as shown in Figure 15. However, real silicon dioxide and especially materials like off-stoichiometric oxide would have a high density of defects. In reality, materials defects are produced because oxygen atoms can be bonded together or they are gone in the tetrahedral structure. The same can be said for the silicon atoms [52, 53]. Generically they are known as point defects.

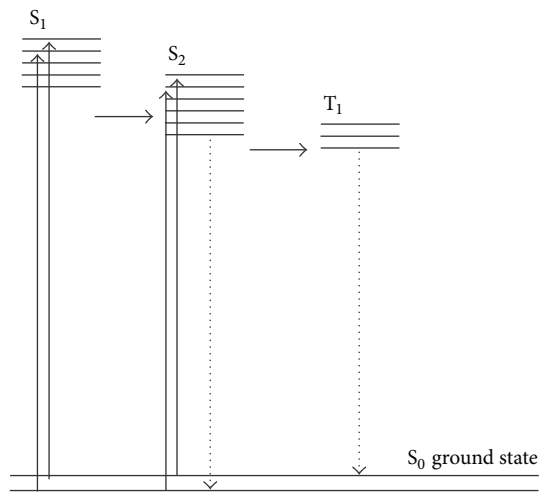


FIGURE 16: Energy interactions allowed in a point defect. Absorption of a photon (solid arrow) from the ground state to a single S_1 produces an electron that rapidly relaxes by internal conversion to a lower vibrational energy (horizontal arrow). Next, it can decay to the S_0 singlet emitting a photon (dotted arrow) or it can relax to the triplet T_1 . It is also possible that the decay to the ground state does not produce an emission.

With quartz being the crystalline and purest form of SiO_2 , it has been used to study the different point defects related to the absorption and emission of light in silicon oxide and electronic structure. So, a parabolic distribution of electronic states related to the molecular vibration has been established [60, 61], and some photon-electron interactions have been proposed [53, 61]. Figure 16 shows some transition allowed in point defects.

Point defects are studied mainly by resonance spectroscopy; specifically paramagnetic centers can be determined by this technique. Others, for example, diamagnetic centers, have to be studied using other techniques. Optical absorption and emission are another important way to determine point defects. In [62] techniques as impedance spectroscopy (IS)/four-point dc conductivity, thermogravimetric analysis/coulometric titration, dilatometry, high-temperature Kelvin probe and Kelvin probe force microscopy, scanning tunneling microscopy (STM)/spectroscopy, X-ray photoelectron spectroscopy (XPS), X-ray absorption spectroscopy, secondary ion mass spectroscopy (SIMS), and X-ray and neutron diffraction (XRD) are mentioned to determine different characteristics of point defects.

Paramagnetic point defects in SiO_2 have been acutely studied in relation to light emission in quartz. The E' center, twofold coordinated Si, the neutral oxygen vacancy, and the nonbridging oxygen hole center (NBOHC) are well-known centers related to the emission of light in quartz [54, 55, 57]. The E' center is formed by an unpaired electron in a dangling orbital sp^3 of a three-coordinated Si atom. Represented as $\text{O}=\text{Si}\cdot$, the \equiv denotes the coordinated three oxygen bonds and the \cdot denotes the unpaired electron. The neutral oxygen vacancy is formed when one oxygen atom is missing and two silicon atoms are directly bonded. Then, it is described

as $\text{O}=\text{Si}-\text{Si}=\text{O}$. The two coordinated Si are represented by $\text{O}-\ddot{\text{Si}}-\text{O}$ where $(\ddot{\cdot})$ represents two paired electrons in the same orbital.

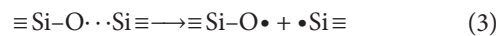
Figure 17 presents different point defects that have been determined by electron spin resonance (ESR). A detailed analysis of the E' center in its different variation is found in [56]. ESR, as its name states, is the magnetic field frequency at which resonance occurs, and the resonance is determined exclusively for each paramagnetic center [52]. The oxygen deficient center in general can be positively or negatively charged, allowing specific optical absorption and electronic transitions.

Also diamagnetic defects, such as neutral oxygen vacancies ($\equiv\text{Si}-\text{Si}\equiv$), two-coordinated silicon atoms ($\text{O}-\text{Si}-\text{O}-$), and peroxy linkages ($\equiv\text{Si}-\text{O}-\text{O}-\text{Si}\equiv$) could be found in quartz. The diamagnetic defects also have absorption optical bands associated with electron transitions [55].

A recent study on generation of color centers deals with the kinetics and growth of defects in silica. In [63] the generation due to heavy ion impact is presented. They use bromide ions accelerated with 5 MV. The evolution of NBOHC, E' , and the oxygen deficient center was studied using the optical absorption characteristic in the visible and UV range. The authors show that the kinetic of the color centers follows the Poisson law.

New advances in the detection system have improved the characterization of defects. Reference [64] presents the diffusion and clustering of the E' centers in quartz; the author shows 2D images of SPR (surface plasmon resonance) portraying the variation in the cluster after different heat treatments. The defects do not follow simple diffusion laws, and they try to stay in the high density areas.

In Silicon Rich Oxide, most of the work has been centered on thermal silicon dioxide implanted with different materials, mainly silicon; see, for example, [58, 65]. The second reference is a very interesting paper and includes, besides the Si implantation, studies on SRO obtained by reactive sputtering of SiO and O. The authors accepted that some cathode luminescence emission bands are related to defects: NBOHC with 650 nm (1.9 eV) red-luminescence, the blue and UV bands 460 and 290 nm (2.7 and 4.3 eV) with the Si related oxygen deficient center (Si-ODC). They also proposed that in absence of H, stressed or weak bonds ($\cdot\cdot\cdot$) could be the precursors of defects and proposed the following equation:



This study included different implantation doses to produce SiO_x with x varying between 0 and 2. Besides, annealing at different temperatures and how these two parameters influence the emission were also presented. In this study Fourier Transform Infrared (FTIR) was used to calibrate the stoichiometry of the layer with a threshold value of x where the emission can be clearly observed. They also proposed that the thermal annealing promotes the rearrangement of the silicon atoms in small clusters as chains or rings within the SiO_x network. The arrangements can be separated into cores of silicon-silicon bonds and the surface where both silicon

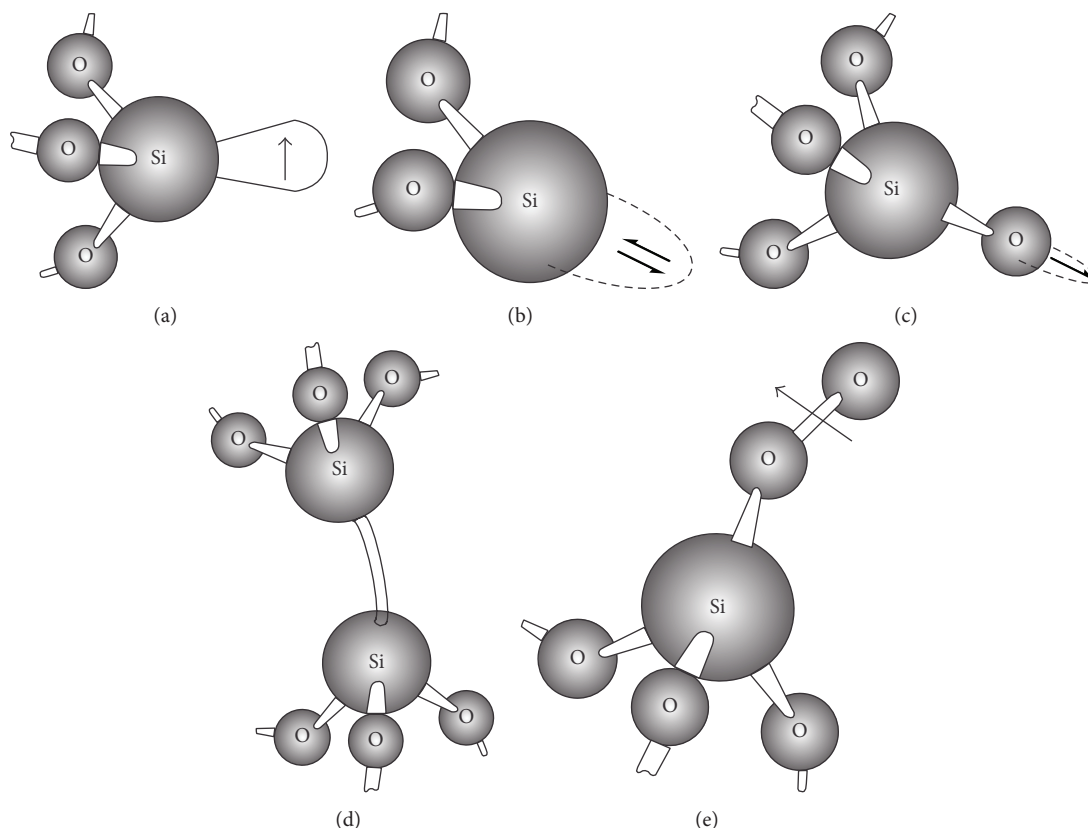


FIGURE 17: Paramagnetic point defects in SiO₂. (a) The E' center [54–56], (b) twofold coordinated silicon [53], (c) nonbridging oxygen hole center (NBOHC) [55], (d) the neutral oxygen vacancy, and (e) peroxy radical [53, 56]. All of these are well-known centers related to the emission of light in quartz [57].

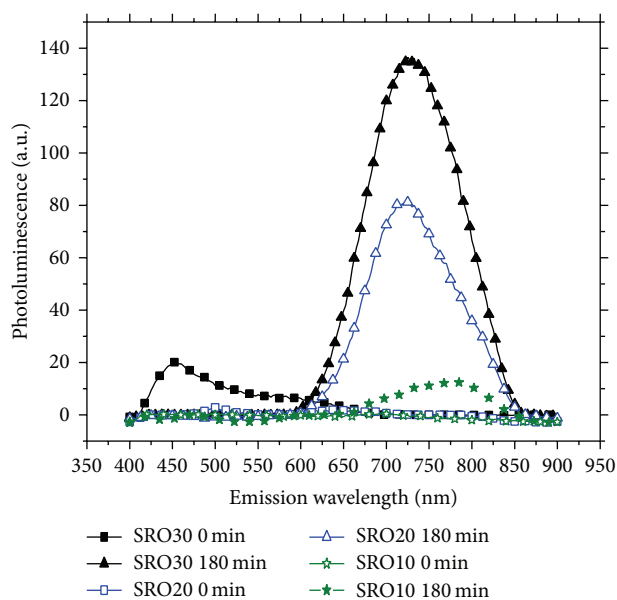


FIGURE 18: PL intensity from samples of SRO deposited by LPCVD as deposited and after annealing at 1100°C. Deposited films have a weak emission; however, after annealing at 1100°C, the PL increases especially for the off-stoichiometric layer with silicon excess lower than 8% ($R_o = 20$ and 30).

and oxygen have dangling bonds. They observed that large extended cluster reduces the luminescence.

The most common technique to obtain SRO is the CVD in its different forms; perhaps it is the most studied together with silicon implantation in thermal oxide. In particular, LPCVD is characterized by deposition at high temperatures in order to dissociate the reactive gases. For example, silane (SiH₄) and nitrous oxide (N₂O) and temperatures of at least of 700°C are used regularly. Under such conditions and during the deposition, many reactions take place and a variety of Si–O bonds are expected [66]. As deposited, the films scarcely have emission but after high temperature treatments, intense emission is developed as shown in Figure 18. This indicates that films obtained by LPCVD are full of defects and that after annealing they become precursors of efficient emissive centers.

As previously mentioned, Si implanted SiO₂ films annealed at a high temperature have emission. However, only those with high implantation dose at around 10¹⁷ atoms/cm² have emission. Berman et al. experimented combining the high silicon excess obtained in a simple way using LPCVD and that obtained by ion implantation [67]. In this study, the SRO films of different silicon concentrations were enriched through silicon implantation. Unexpectedly, the results show that the highest emission was obtained in films with low

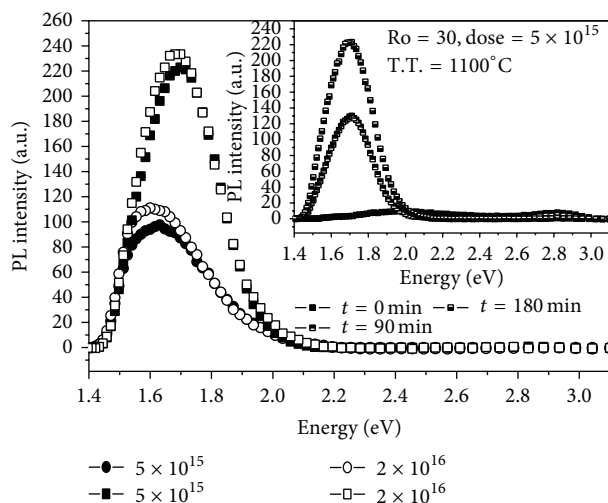


FIGURE 19: PL intensity from SRO films super enriched with silicon implantation [58]. $R_o = 20$ and 30 correspond to a silicon excess of around 5 to 7%, denoted by squares and circles, respectively. The PL intensity increased after thermal annealing at 1100°C during 180 min, as shown in the inset.

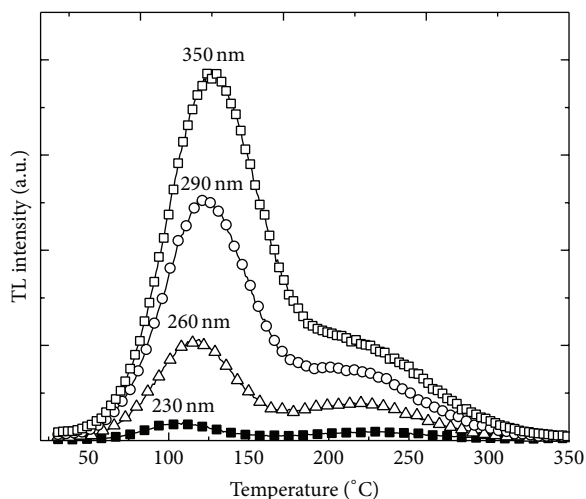


FIGURE 20: Thermo-luminescent emission induced by UV irradiation of samples SRO20 obtained by LPCVD after 1100°C annealing [59]. The wavelength used to charge the traps is shown in each curve; as the photon energy increases, the thermoluminescent emission reduces.

silicon excess. As shown in Figure 19, Si implantation with a dose as low as $1 \times 10^{15} \text{ at-cm}^{-2}$ and silicon excess as low as 5% deposited by LPCVD generates, after annealing, high photoluminescence.

DiMaria et al. observed electroluminescence in films obtained by LPCVD. However, they divided the films into SRO and off-stoichiometric silicon oxides (OSO) according to the silicon excess. Low silicon excess, say less than 7%, represented by $R_o \geq 20$ is OSO, and high silicon

excess, say more than 10% and represented by $R_o \leq 10$, is SRO [68, 69]. The deposited SRO has many silicon nanocrystals and the density increases rapidly when the films are subjected to high temperature annealing. However, neither DiMaria nor our group found Sinc in OSO [68, 70].

In [67] FTIR studies of SRO and OSO demonstrate that the stretching frequency increases after annealing for all silicon excess. This result suggests a phase separation during the thermal annealing and then an increase of oxidized compounds. Moreover, they include XPS studies showing that after annealing at 1100°C a phase separation of elemental silicon, non stoichiometric silicon oxide and SiO_2 , is produced; for low silicon excess the SiO_x phase dominates. They conclude that two competitive morphological mechanisms take place during annealing: one is the formation of silicon agglomerates and the other is the formation of silicon and oxygen compounds. If silicon excess is high enough, the silicon agglomerates will form into nanocrystals. As Si content is decreased, however, silicon oxidation states will dominate due to the larger separation between elemental silicons. As silicon excess increases, the SRO will tend towards a polysilicon layer; conversely, as silicon is reduced, the SRO film will move towards a stoichiometric SiO_2 . In between these extremes, agglomeration of silicon shifts towards the agglomeration of Si-oxygen compounds as the silicon excess moves from high to low silicon excess.

Thermoluminescence, TL, is a technique similar to PL; in this case, temperature is used instead of light. TL is mostly used in anthropology in the dating of antique objects. The principle involved in this technique is that some materials, after exposure to radiation (e.g., sun light) store charges due to defects. Then, when they are heated the electrons are released and they recombine emitting light [71, 72]. While this technique can be used to study emission in materials damaged by radiation such as quartz, few reports can be found in the literature on this subject [73], and even less for SRO or for OSO. Piters et al. present a study of thermoluminescence found in SRO [59]; the spectrum of emission is shown in Figure 20 where the emitted wavelength is not determined. However, the intensity of the emission depends on the radiation used to charge the sample. However, a model is proposed that deals with charge trapped in acceptor traps and their emitting decay after heating.

Cathodo- and electroluminescence, CL and EL, are used to determine the emissive centers that cannot be excited in PL and also all the emissive electronic states can be reached [74]. In both techniques, electrons are injected into the conduction band of the material so that more energetic traps can be reached. CL and EL have been used to study the emission of SRO where electrons are injected into the film by a high acceleration field or by biasing the sample with a voltage [70, 75, 76]. Figure 21 shows the whole range of emissions of OSO that goes from 400 to 850 nm; PL only emits in a short part of the spectrum. The most energetic technique is CL which produces a spectrum within the more energetic side of the spectrum. EL emission increases

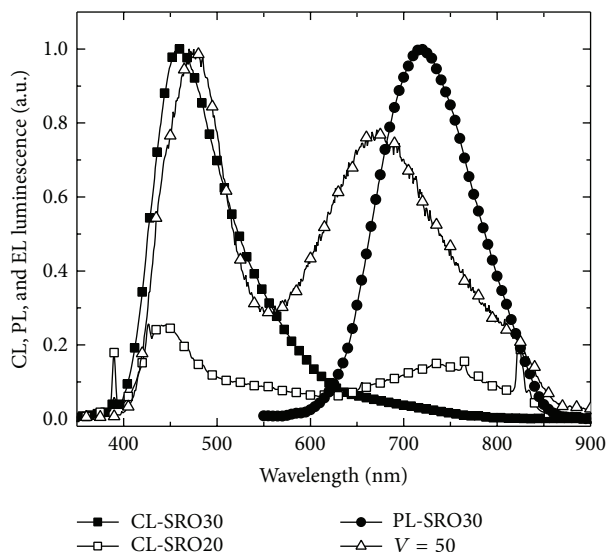


FIGURE 21: Photo-, cathodo-, and electroluminescence behavior of OSO films deposited by LPCVD; EL was biased by 50 volts. It is clear that CL and EL include the PL, and the full emission range is from 400 to 450 nm. As the bias voltage increases, the EL blue peak increases more than the red one and the EL spectrum tends towards that of the CL.

as more voltage is applied; that is, as the energy increases the emission shifts to that of the CL. In the references mentioned, because of the lack of nanocrystals, the authors conclude that the whole range of emission is due to Si–O compounds. All of these emissions are characteristics of Si–O defects [77, 78]. So, we can say that OSO is a material that emits basically by point defect centers, either individually or forming chains or rings. However, in spite of that, OSO can be considered as a reference material where the emission is due to defect center. To our knowledge there is no study relating the emission with paramagnetic or diamagnetic centers.

4. Conclusions

In summary, different models have been published to explain the physical mechanisms underlying the luminescent emission of Sinc-based materials and, specifically, those related to Sinc core, to Sinc/SiO₂ interface, and to the SiO₂ matrix. As common characteristics to most of them, we distinguish the following: (i) there is a key role to the interface between the silicon (core) and the silicon oxide, (ii) the light absorption takes place in the nanometer-sized core following a quantum confinement effect whereas the (radiative) recombination occurs at the interface, and (iii) the quantum size phenomenon is the basic emission mechanism, in a definite range of the luminescence spectral distribution, when the materials are obtained, posttreated, and measured under definite conditions.

For these materials and concerning Sinc core and Sinc surface, two main PL bands should be considered: slow decay band (microsecond time scale) and a discrete fast blue band

(nanosecond time scale). The spectral behavior of the first band depends on the electronic states on Sinc/surface. For H-passivated Sinc, this band continuously varies from infrared to ultraviolet as Sinc size decreases according to the quantum confinement effect. On the contrary, for oxidized Sinc-based materials, the band pins at about 1.7 eV if the oxidation has taken place at an elevated temperature and at about 2.1 eV if it has been achieved at room temperature in free atmosphere due to differences in the oxygen passivation configurations.

Concerning the SiO₂ matrix, emission is basically related to different point defects both paramagnetic and diamagnetic. Paramagnetic defects have been well established in quartz using resonance techniques. However, diamagnetic defects are more difficult to determine and other techniques have been proposed to study them. The E' center, twofold coordinated Si, the neutral oxygen vacancy, and the nonbridging oxygen hole center (NBOHC) are well known centers related to the emission of light in quartz. Also, diamagnetic defects, for example, neutral oxygen vacancies ($\equiv\text{Si}-\text{Si}\equiv$), two-coordinated silicone atoms ($\text{O}-\text{Si}-\text{O}-$), and peroxy linkages ($\equiv\text{Si}-\text{O}-\text{O}-\text{Si}\equiv$), could be found in quartz and determined optically. The emission range observed in the point defects goes from UV to the near infrared. Also, the CVD deposition technique, especially LPCVD, is used to obtain the SRO and OSO that tends to produce many defects; it is likely that the light emission in the range from 400 to 850 nm is due mostly to point defects.

Conflict of Interests

The authors declare that there is no conflict of interests regarding the publication of this paper.

Acknowledgments

The authors appreciate the English revision done by Rebekah Hosse Clark. Also, the authors appreciate the support of CONACyT.

References

- [1] L. T. Canham, "Silicon quantum wire array fabrication by electrochemical and chemical dissolution of wafers," *Applied Physics Letters*, vol. 57, no. 10, p. 1046, 1990.
- [2] F. Koch and V. Petrova-Koch, "Light from Si-nanoparticle systems—a comprehensive view," *Journal of Non-Crystalline Solids*, vol. 198–200, no. 2, pp. 840–846, 1996.
- [3] F. Iacona, G. Franzò, and C. Spinella, "Correlation between luminescence and structural properties of Si nanocrystals," *Journal of Applied Physics*, vol. 87, no. 3, pp. 1295–1303, 2000.
- [4] F. Iacona, C. Spinella, S. Boninelli, and F. Priolo, "Formation and evolution of luminescent Si nanoclusters produced by thermal annealing of films," *Journal of Applied Physics*, vol. 95, p. 3723, 2004.
- [5] A. Uhler, "Electrolytic shaping of germanium and silicon," *The Bell System Technical Journal*, vol. 35, no. 2, pp. 333–347, 1956.
- [6] M. A. Tischler, R. T. Collins, J. H. Stathis, and J. C. Tsang, "Luminescence degradation in porous silicon," *Applied Physics Letters*, vol. 60, no. 5, pp. 639–641, 1992.

- [7] I. M. Chang, S. C. Pan, and Y. F. Chen, "Light-induced degradation on porous silicon," *Physical Review B*, vol. 48, no. 12, pp. 8747–8750, 1993.
- [8] K. Dohnalová, L. Ondic, K. Kúsová, I. Pelant, J. L. Rehspringer, and R.-R. Mafouana, "White-emitting oxidized silicon nanocrystals: discontinuity in spectral development with reducing size," *Journal of Applied Physics*, vol. 107, no. 5, Article ID 053102, 22 pages, 2010.
- [9] C.-C. Tu, Q. Zhang, L. Y. Lin, and G. Cao, "Brightly photoluminescent phosphor materials based on silicon quantum dots with oxide shell passivation," *Optics Express*, vol. 20, no. 1, pp. A69–A74, 2012.
- [10] C. Lin and G. Lin, "Defect-enhanced visible electroluminescence of multi-energy silicon-implanted silicon dioxide film," *IEEE Journal of Quantum Electronics*, vol. 41, no. 3, pp. 441–447, 2005.
- [11] R. J. Walters, J. Kalkman, A. Polman, H. A. Atwater, and M. J. A. de Dood, "Photoluminescence quantum efficiency of dense silicon nanocrystal ensembles in SiO₂," *Physical Review B*, vol. 73, Article ID 132302, 2006.
- [12] T. S. Iwayama, T. Hama, D. E. Hole, and I. W. Boyd, "Enhanced luminescence from encapsulated silicon nanocrystals in SiO₂ with rapid thermal anneal," *Vacuum*, vol. 81, no. 2, pp. 179–185, 2006.
- [13] H. Z. Song, X. M. Bao, N. S. Li, and J. Y. Zhang, "Relation between electroluminescence and photoluminescence of Si⁺-implanted SiO₂," *Journal of Applied Physics*, vol. 82, no. 8, Article ID 4028, 5 pages, 1997.
- [14] A. Morales, J. Barreto, C. Domínguez, M. Riera, M. Aceves, and J. Carrillo, "Comparative study between silicon-rich oxide films obtained by LPCVD and PECVD," *Physica E*, vol. 38, p. 54, 2007.
- [15] M. Aceves-Mijares, A. A. González-Fernández, R. López-Estopier et al., "On the origin of light emission in silicon rich oxide obtained by low-pressure chemical vapor deposition," *Journal of Nanomaterials*, vol. 2012, Article ID 890701, 11 pages, 2012.
- [16] X. Y. Chen, Y. Lu, L. Tang et al., "Thermal-wave nondestructive evaluation of cylindrical composite structures using frequency-domain photothermal radiometry," *Journal of Applied Physics*, vol. 97, pp. 014911–014913, 2005.
- [17] J. Barreto, M. Perálvarez, J. A. Rodríguez et al., "Pulsed electroluminescence in silicon nanocrystals-based devices fabricated by PECVD," *Physica E*, vol. 38, pp. 193–196, 2007.
- [18] G. D. Sorarù, S. Modena, P. Bettotti, G. Das, G. Mariotto, and L. Pavesi, "Si nanocrystals obtained through polymer pyrolysis," *Applied Physics Letters*, vol. 83, no. 4, pp. 749–751, 2003.
- [19] G. Das, L. Ferraioli, P. Bettotti et al., "Si-nanocrystals/SiO₂ thin films obtained by pyrolysis of sol-gel precursors," *Thin Solid Films*, vol. 516, no. 20, pp. 6804–6807, 2008.
- [20] J. A. Rodríguez, C. Fernández Sánchez, C. Domínguez, S. Hernández, and Y. Berencén, "Bulk silica-based luminescent materials by sol-gel processing of non-conventional precursors," *Applied Physics Letters*, vol. 101, no. 17, Article ID 171908, 2012.
- [21] S. T. H. Silalahi, H. Y. Yang, K. Pita, and Y. Mingbin, "Rapid thermal annealing of sputtered silicon-rich oxide/SiO₂ superlattice structure," *Electrochemical and Solid-State Letters*, vol. 12, no. 4, pp. K29–K32, 2009.
- [22] S. J. Huang and G. Conibeer, "Sputter-grown Si quantum dot nanostructures for tandem solar cells," *Journal of Physics D: Applied Physics*, vol. 46, no. 2, Article ID 024003, 2013.
- [23] D. Y. Shin, J. H. Park, S. Kim, S. Choi, and K. J. Kim, "Graded-size Si-nanocrystal-multilayer solar cells," *Journal of Applied Physics*, vol. 112, no. 10, Article ID 104304, 2012.
- [24] V. Lehmann and U. Gosele, "Porous silicon formation: a quantum wire effect," *Applied Physics Letters*, vol. 58, no. 8, p. 856, 1991.
- [25] W. Wu, X. F. Huang, L. J. Chen et al., "Room temperature visible electroluminescence in silicon nanostructures," *Journal of Vacuum Science & Technology A*, vol. 17, no. 1, pp. 159–163, 1999.
- [26] C. Delerue, G. Allan, and M. Lannoo, "Theoretical aspects of the luminescence of porous silicon," *Physical Review B*, vol. 48, no. 15, pp. 11024–11036, 1993.
- [27] A. D. Yoffe, "Low-dimensional systems: quantum size effects and electronic properties of semiconductor microcrystallites (zero-dimensional systems) and some quasi-two-dimensional systems," *Advances in Physics*, vol. 42, pp. 173–262, 1993.
- [28] T. Takagahara and K. Takeda, "Theory of the quantum confinement effect on excitons in quantum dots of indirect-gap materials," *Physical Review B*, vol. 46, no. 23, pp. 15578–15581, 1992.
- [29] A. Gupta, M. T. Swihart, and H. Wiggers, "Luminescent colloidal dispersion of silicon quantum dots from microwave plasma synthesis: exploring the photoluminescence behavior across the visible spectrum," *Advanced Functional Materials*, vol. 19, no. 5, pp. 696–703, 2009.
- [30] B. Garrido Fernandez, M. López, C. García et al., "Influence of average size and interface passivation on the spectral emission of Si nanocrystals embedded in SiO₂," *Journal of Applied Physics*, vol. 91, no. 2, pp. 798–807, 2002.
- [31] L. W. Wang and A. Zunger, "Electronic structure pseudopotential calculations of large (approximately 1000 atoms) Si quantum dots," *Journal of Physical Chemistry*, vol. 98, no. 8, pp. 2158–2165, 1994.
- [32] I. Sychugov, R. Juhasz, J. Valenta, and J. Linnros, "Narrow luminescence linewidth of a silicon quantum dot," *Physical Review Letters*, vol. 94, no. 8, Article ID 087405, 2005.
- [33] J. P. Wilcoxon, G. A. Samara, and P. N. Provencio, "Optical and electronic properties of Si nanoclusters synthesized in inverse micelles," *Physical Review B: Condensed Matter and Materials Physics*, vol. 60, no. 4, pp. 2704–2714, 1999.
- [34] T. Torchynska, F. G. Becerril Espinoza, Y. Goldstein et al., "Nature of visible luminescence of co-sputtered Si-SiO_x systems," *Physica B*, vol. 340–342, pp. 1119–1123, 2003.
- [35] Y. Kanemitsu, H. Uto, Y. Masumoto, T. Matsumoto, T. Futagi, and H. Mimura, "Microstructure and optical properties of free-standing porous silicon films: size dependence of absorption spectra in Si nanometer-sized crystallites," *Physical Review B*, vol. 48, no. 4, pp. 2827–2830, 1993.
- [36] S. M. Prokes, "Light emission in thermally oxidized porous silicon: evidence for oxide-related luminescence," *Applied Physics Letters*, vol. 62, p. 3244, 1993.
- [37] V. Petrova-Koch, T. Muschik, A. Kux, B. K. Meyer, F. Koch, and V. Lehmann, "Rapid-thermal-oxidized porous Si-the superior photoluminescent Si," *Applied Physics Letters*, vol. 61, no. 8, pp. 943–945, 1992.
- [38] M. V. Wolkin, J. Jorne, P. M. Fauchet, G. Allan, and C. Delerue, "Electronic states and luminescence in porous silicon quantum dots: The role of oxygen," *Physical Review Letters*, vol. 82, no. 1, pp. 197–200, 1999.

- [39] Y. Kanemitsu, T. Ogawa, K. Shiraishi, and K. Takeda, "Visible photoluminescence from oxidized Si nanometer-sized spheres: exciton confinement on a spherical shell," *Physical Review B*, vol. 48, no. 7, pp. 4883–4886, 1993.
- [40] P. T. Huy and P. H. Duong, "Intense photoluminescence and photoluminescence enhancement of silicon nanocrystals by ultraviolet irradiation," *Advanced Materials Research*, vol. 31, pp. 74–76, 2007.
- [41] L. Khomenkova, N. Korsunska, V. Yukhimchuk et al., "Nature of visible luminescence and its excitation in Si-SiO_x systems," *Journal of Luminescence*, vol. 102–103, pp. 705–711, 2003.
- [42] M. S. Brandt, H. D. Fuchs, M. Stutzmann, J. Weber, and M. Cardona, "The origin of visible luminescence from "porous silicon": a new interpretation," *Solid State Communications*, vol. 81, no. 4, pp. 307–312, 1992.
- [43] S. M. Prokes, O. J. Glemboki, V. M. Bermudez, R. Kaplan, L. E. Friedersdorf, and P. C. Searson, "SiH_x excitation: an alternate mechanism for porous Si photoluminescence," *Physical Review B*, vol. 45, no. 23, pp. 13788–13791, 1992.
- [44] Y. Kanemitsu, "Luminescence properties of nanometer-sized Si crystallites: core and surface states," *Physical Review B*, vol. 49, no. 23, pp. 16845–16848, 1994.
- [45] M. Nishida, "Calculations of the electronic structure of silicon quantum dots: oxidation-induced redshifts in the energy gap," *Semiconductor Science and Technology*, vol. 21, pp. 443–449, 2006.
- [46] K. Takeda and K. Shiraishi, "Electronic structure of silicon-oxygen high polymers," *Solid State Communications*, vol. 85, no. 4, pp. 301–305, 1993.
- [47] F. Koch and V. Petrova-Koch, "The surface state mechanism for light emission from porous silicon," *Porous Silicon*, pp. 133–147, 1994.
- [48] F. Koch, "Models and mechanisms for the luminescence of Porous Si," *MRS Proceedings*, vol. 298, p. 319, 1993.
- [49] F. Koch, V. Petrova-Koch, and T. Muschik, "The luminescence of porous Si: the case for the surface state mechanism," *Journal of Luminescence*, vol. 57, no. 1–6, pp. 271–281, 1993.
- [50] D. I. Kovalev, I. D. Yaroshetzki, T. Muschik, V. Petrova-Koch, and F. Koch, "Fast and slow visible luminescence bands of oxidized porous Si," *Applied Physics Letters*, vol. 64, no. 2, pp. 214–216, 1994.
- [51] H. Yu, J.-Q. Zeng, and Z.-R. Qiu, "Silicon nanocrystals," in *Crystalline Silicon—Properties and Uses*, S. Basu, Ed., InTech, Hampshire, UK, 2011.
- [52] D. L. Griscom, "Optical properties and structure of defects in silica glass," *Journal of the Ceramic Society of Japan*, vol. 99, no. 1154, pp. 923–942, 1991.
- [53] L. Skuja, "Optically active oxygen-deficiency-related centers in amorphous silicon dioxide," *Journal of Non-Crystalline Solids*, vol. 239, no. 1–3, pp. 16–48, 1998.
- [54] R. A. Weeks, "Paramagnetic spectra of E₂' centers in crystalline quartz," *Physical Review*, vol. 130, no. 2, pp. 570–576, 1963.
- [55] R. Salh, "Defect related luminescence in silicon dioxide network: a review," in *Crystalline Silicon—Properties and Uses*, S. Basu, Ed., chapter 8, pp. 135–172, InTech, 2011.
- [56] E. H. Poindexter and W. L. Warren, "Paramagnetic point defects in amorphous thin films of SiO₂ and Si₃N₄: updates and additions," *Journal of the Electrochemical Society*, vol. 142, no. 7, pp. 2508–2516, 1995.
- [57] E. P. O'Reilly and J. Robertson, "Theory of defects in vitreous silicon dioxide," *Physical Review B*, vol. 27, no. 6, pp. 3780–3795, 1983.
- [58] H. Fitting, T. Barfels, A. N. Trukhin, B. Schmidt, A. Gulans, and A. von Czarnowski, "Cathodoluminescence of Ge⁺, Si⁺, and O⁺ implanted SiO₂ layers and the role of mobile oxygen in defect transformations," *Journal of Non-Crystalline Solids*, vol. 303, no. 2, pp. 218–231, 2002.
- [59] T. M. Pitters, M. Aceves, D. Berman-Mendoza, L. R. Berriel-Valdos, and J. A. Luna-López, "Dose dependent shift of the TL glow peak in a silicon rich oxide (SRO) film," *Revista Mexicana de Física S*, vol. 57, no. 2, pp. 26–29, 2011.
- [60] J. S. Shie, "The absorption band shape of color centers with many-mode interaction," *Chinese Journal of Physics*, vol. 15, no. 1, pp. 23–28, 1977.
- [61] M. Cannas, *Point defects in amorphous SiO₂: optical activity in the visible, UV and vacuum-UV spectral regions* [Ph.D. thesis], Università Degli Studi Di Palermo, 1998.
- [62] H. L. Tuller and S. R. Bishop, "Point defects in oxides: tailoring materials through defect engineering," *Annual Review of Materials Research*, vol. 41, pp. 369–398, 2011.
- [63] J. Manzano-Santamaría, J. Olivares, A. Rivera, O. Peña-Rodríguez, and F. Agulló-López, "Kinetics of color center formation in silica irradiated with swift heavy ions: thresholding and formation efficiency," *Applied Physics Letters*, vol. 101, no. 15, Article ID 154103, 4 pages, 2012.
- [64] E. Suhovoy, V. Mishra, M. Shklyar, L. Shtirberg, and A. Blank, "Direct micro-imaging of point defects in bulk SiO₂, applied to vacancy diffusion and clustering," *Europhysics Letters*, vol. 90, no. 2, Article ID 26009, 2010.
- [65] R. Salh, "Nanocluster in silicon dioxide: cathodoluminescence, energy dispersive X-ray analysis and infrared spectroscopy studies," in *Crystalline Silicon—Properties and Uses*, S. Basu, Ed., InTech, 2011.
- [66] A. Sherman, *Chemical Vapor Deposition for Microelectronics: Principles, Technology, and Applications*, Noyes Publications, Park Ridge, NJ, USA, 1987.
- [67] D. Berman, M. Aceves, A. Gallegos et al., "Silicon excess and thermal annealing effects on the photoluminescence of SiO₂ and silicon rich oxide super enriched with silicon implantation," *Physica Status Solidi C*, vol. 1, pp. S83–S87, 2004.
- [68] D. J. DiMaria, J. R. Kirtley, E. J. Pakulis et al., "Electroluminescence studies in silicon dioxide films containing tiny silicon islands," *Journal of Applied Physics*, vol. 56, no. 2, pp. 401–416, 1984.
- [69] D. Dong, E. A. Irene, and D. R. Young, "Preparation and some properties of chemically vapor-deposited Si-rich SiO₂ and Si₃N₄ films," *Journal of The Electrochemical Society*, vol. 125, pp. 819–823, 1978.
- [70] M. Aceves-Mijares, A. A. González-Fernández, R. López-Estopier et al., "On the origin of light emission in silicon rich oxide obtained by low-pressure chemical vapor deposition," *Journal of Nanomaterials*, vol. 2012, Article ID 890701, 11 pages, 2012.
- [71] D. Richter, "Advantages and limitations of thermoluminescence dating of heated flint from paleolithic sites," *Geoarchaeology*, vol. 22, no. 6, pp. 671–683, 2007.
- [72] Z. Jacobs and R. G. Roberts, "Advances in optically stimulated luminescence dating of individual grains of quartz from archaeological deposits," *Evolutionary Anthropology*, vol. 16, no. 6, pp. 210–223, 2007.
- [73] T. W. Hickmott, "Thermoluminescence and color centers in rf-sputtered SiO₂ films," *Journal of Applied Physics*, vol. 43, no. 5, p. 2339, 1972.

- [74] B. G. Yacobi and D. B. Holt, *Cathodoluminescence Microscopy of Inorganic Solids*, Springer, New York, NY, USA, 1990.
- [75] R. López-Estopier, M. Aceves, Z. Yu, and C. Falcony, "Determination of the energy states of the donor acceptor decay emission in silicon rich oxide prepared by low-pressure chemical vapor deposition," *Journal of Vacuum Science and Technology B*, vol. 29, no. 2, Article ID 021017, 2011.
- [76] R. López-Estopier, M. Aceves, and C. Falcony, "Cathodo- and photo-luminescence of silicon rich oxide films obtained," in *Cathodoluminescence*, N. Yamamoto, Ed., pp. 978–953, InTech, 2012.
- [77] L. Skuja, K. Kajihara, M. Hirano, and H. Hosono, "Visible to vacuum-UV range optical absorption of oxygen dangling bonds in amorphous SiO₂," *Physical Review B: Condensed Matter and Materials Physics*, vol. 84, no. 20, Article ID 205206, 2011.
- [78] M. Cannas, "Luminescence properties of point defects in silica," in *GNSR 2001: State of Art and Future Development in Raman Spectroscopy and Related Techniques*, G. Messina and S. Santangelo, Eds., IOS Press, 2002.

